Asian Journal of Physics
Vol. 33, Nos 3 & 4 (2024) 253-268
Available on: www.asianjournalofphysics.com

ap

Cavity opto-mechanics in whispering gallery mode resonators: Route to chaos

Gabriele Frigenti, Daniele Farnesi, Stefano Pelli, Gualtiero Nunzi Conti, and Silvia Soria

CNR-IFAC Institute of Applied Physics "N.Carrara", 50019 Sesto Fiorentino, Italy

Dedicated to Professor Anna Consortini for her significant contributions and pioneering works in the field of atmospheric turbulence and her continuous commitment to promote optics at global level

This paper reviews the different mechanical dynamics in whispering gallery mode resonators (toroids, microspheres and microbubbles) generated by radiation pressure. The emergence of chaotic motion is shown in different geometries as it is an intrinsic property of the optical microcavities. The different routes to chaos are described and they include period doubling, aperiodic motion and complex trajectories.

Doi: 10.54955/AJP.33.3-4.2024.253-268

Keywords: Whispering gallery mode, Chaotic motion, Optical microcavities.

1 Introduction

In 1960 with the birth of the laser source [1] a door opened on new scientific discoveries and advancements. In 1961, nonlinear optical processes were demonstrated: the first one was second harmonic generation [2] followed very closely by other frequency conversion processes [3,4]. The high intensity laser light has facilitated the study of many novel nonlinear optical phenomena [5-7]. Usually, nonlinear optical phenomena have been observed in combination of pulsed laser sources, anomalous dispersion, high nonlinear coefficients or long interaction lengths. Another way of generating nonlinear phenomena is resorting to optical resonators and, among them, whispering gallery mode resonators (WGMR) have attracted significant attention [8,9].

A whispering gallery is defined by the Oxford dictionary as "a gallery or dome with acoustic properties such that a faint sound may be heard round its entire circumference". Whispering gallery modes were first discovered by Lord Rayleigh in Saint Paul's cathedral in London [10]. This acoustic phenomenon can be applied to optics: an optical wave can be totally internally reflected while traveling around a circular medium. In general, two types of materials are used to fabricate optical whispering gallery mode resonators: semiconductors, which allows the use of advanced fabrications techniques and therefore to realise with precision sub-micrometic structures, and glasses, which allow to minimize the absorption losses and obtain the best optical performances.

In this Review we will focus on whispering gallery resonators, which are fabricated with glasses such as fused silica. WGMR can sustain mechanical oscillations due to radiation pressure, which compete with the non-linear frequency generation [11,12].

2 Whispering gallery mode resonators overview

There is a wide variety of systems that can support optical WGMs, such as microspheres, microdisks, microtoroids, microrings and micropillars. In addition, WGMs are sustained even by hollow structures, such as microbubbles and microbottles, or by liquid structures, such as the microdroplets [13,14]. In all cases,

Corresponding author
e mail: S.Soria@ifac.cnr.it (Silvia Soria)

the systems present a cylindrical symmetry around one axis, have curved dielectric surfaces and present a high refractive index contrast with the surrounding medium. These features allow the formation of the optical WGMs, which are produced by the combination of the total internal refraction and the guiding effect provided by the curved interfaces. As consequence, WGMs are concentrated in close proximity to the dielectric interfaces ("wall sticking"), while running circular paths around the symmetry axis. In this regard, WGMs can be easily and effectively visualised as rings of light localised at the dielectric boundaries. The small size of the WGMRs, the sharpness of their optical spectrum and, for specific applications, even their mechanical properties make WGMRs excellent candidates for the integration in complex photonic devices.

From a formal point of view, WGMs are found as solutions of the vectorial Helmholtz equations after the application of appropriate boundary conditions on both the electric and the magnetic fields. In particular, this resolution defines both the resonance wavelengths of the WGMs as well as their spatial distributions. As a general feature, WGMs are mostly localised within the resonator physical boundary (i.e. within the dielectric surfaces), but they also have a very small fraction extending in the surrounding environment as evanescent tails. These evanescent tails play an important role since they allow to couple the WGMs to an external waveguide and then inject and/or extract light from the WGMs. There are different waveguides and strategies that can be implemented to achieve the WGM-waveguide coupling, but all implementation shares two main goals: achieving both a good spatial overlap and phase matching between the WGMs and the waveguide mode.

Once the coupling is achieved, laser light can be injected into the resonator to excite its WGM resonances. By scanning the laser wavelength and recording the system transmission, it is then possible to observe the lineshape of the WGM resonances and define a series of parameters to characterise the resonator. This list of figures-of-merit is inherited from interferometry and comprises, for example, the quality factor Q, the finesse, the contrast (or visibility), the full-width half-maximum (FWHM) and the free spectral range (FSR). Among these parameters, the quality factor Q, the finesse and the contrast are the most important in applications, since they quantify the sharpness of the WGM resonances, the average number of photon round-trips and the loaded energy in the WGM, respectively.

Due to their sharp optical spectrum, their little modal volume and little footprint, WGM resonators have found applications in several fields [15-17] and are also suitable for the design of low threshold lasers [18]. In the last years, a wide range of nonlinear phenomena at room temperature on WGMR have been studied [7]. The unique characteristics of these devices allow to excite and observe optical nonlinear effects and optomechanical effects [19].

3 The microbubble resonator: a hollow spherical WGMR

Microbubble Resonators (MBR) are hollow WGMRs produced by the inflation of a glass capillary. In practical terms, this inflation is achieved by pressuring the capillary with an inert gas (e.g. nitrogen) and then rapidly heating it, through a laser pulse [20] or an electric discharge [21]. This rapid heating produces a softening of the capillary walls, which expand to a spherical bulge due to the internal pressure: this bubble-shaped bulge is the resonator itself. At variance with other WGMRs, MBRs are hollow and can be filled with liquids or gasses through their capillary stem [22-25]. For this reason, MBRs are ideal optical sensors for studying the properties of the hosted fluid, focusing, for example, on its viscosity [24,25], its refractive index [21,23] its photoacoustic properties [26] or its thermal properties [27].

The MBRs used in this study were fabricated with the arc discharge technique described in [21]. They were produced from fused silica capillaries (Z-FSS-200280 and Z-FSS-100165 from Postnova Analytics GmbH, Landsberg, Germany) and their typical radius fell in the (200 μm - 250 μm) range. Panel (a) of Fig 1 shows an MBR mounted on the discharge system after the inflation process. After the fabrication process, the MBR can be characterised by coupling it to a home-made tapered fiber and then scanning its WGM

spectrum through a tunable laser source (Tunics plus, NetTest; spectral range 1500 nm - 1640 nm, in-fiber emission). As shown in Panel (b) of Fig 1 by a representative resonance, the MBR resonances show a high contrast (0.95), a high quality factor Q (6.0×10^6) and a narrow FWHM (32 MHz).

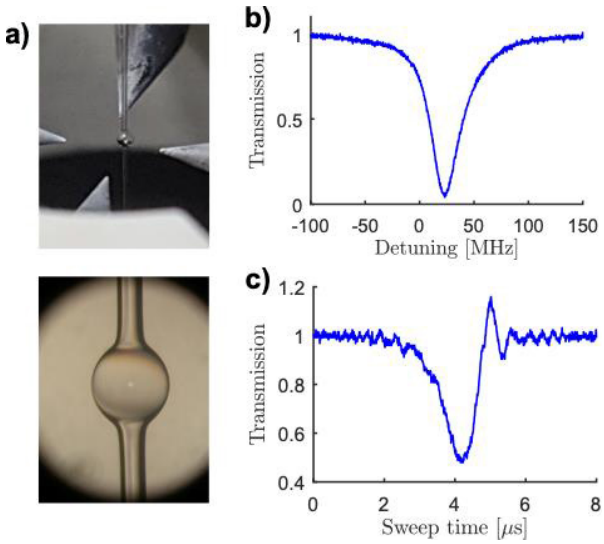

Fig 1. (a) Wide shot showing the MBR and the electrodes used for the arch discharge (top), and microscope image of the MBR (bottom), (b) Typical profile of an MBR resonance, (c) Cavity ring down profile of an MBR resonance.

These promising optical features are a consequence of the little value of the intrinsic losses and the coupling losses of the system as well as their little difference (critical coupling). More in detail, the intrinsic losses are the ones connected with the quality of the fabrication process and account for the absorption of the material making up the MBR, the scattering produced by the roughness of the MBR surface and the contamination of the MBR surface by impurities (e.g. dust). Coupling losses, instead, quantify the energy exchange between the waveguide and the MBR. The above mentioned quantities can be retrieved by performing a fast wavelength scan of the WGM resonance and analysing the resulting cavity ring down (CRD) profile [28]. Panel (c) of Fig 1 shows an example of these CRD profiles, whose analysis leads to round-trip intrinsic losses $\zeta^2 = 2.8\times10^{-5}$ and round-trip coupling losses $k^2 = 6.4\times10^{-6}$, proving the overall small values and little difference. In addition, the intrinsic losses ζ^2 can be used to compute an intrinsic quality factor $Q_0 = 3.3\times10^8$, proving the high quality of the arc discharge fabrication process.

4 Thermal locking technique

For nonlinear applications of WGMRs, the detuning between the laser source and the WGM resonant wavelength needs to be constant (ideally null, for a maximum coupling of energy in the resonator). In this section, we will describe the fundamentals of the thermal locking technique, which enables the stabilisation of this detuning. In contrast with other stabilisation techniques, thermal locking is a passive technique (e.g. there is no feedback action on the laser source) and it has proven to be an efficient method for the excitation and the measurement of all the nonlinear phenomena described in this paper.

In general terms, the high Q factor and the small volume of the WGMs produce large modal intensities and, consequently, the circulating power within the cavity is extremely high even for low input powers. The circulating intensity within the WGMR can be approximated as

$$I = P_{in}\lambda Q / 2\pi n V_{eff}$$

where P_{in} is the coupled input power, λ the laser wavelength, n the refractive index and V_{eff} the mode volume. For a spherically shaped WGMR such as the MBRs of this paper, with a Q factor of about 10^8, a mode volume of about 500 mm^3, and an input power of 1 mW, the circulating power exceeds 1 GW/cm^2 [29].

These huge circulating powers are crucial to observe nonlinear optical phenomena, but they can result in thermal nonlinearities [30]. In particular, even if the material is highly transparent in the wavelength window of interest, a tiny absorption of such high powers can lead to a significant heating of the WGMR. This heating, in turn, induces small variations of the refractive index and/or of the geometrical parameters (e.g. wall thickness, radii, etc...), which result in a red-shift of the resonance. Such shifts cannot be neglected since they can exceed several times the resonance linewidth, and produce deformation of the WGM lineshape during a wavelength scan. In practice, if the WGM resonance is probed through a ``red'' scan (i.e. by sweeping the laser source towards longer wavelengths), the laser light and the resonance move in the same direction, causing a strong broadening of the lineshape. Conversely, in the case of a ``blue'' scan (i.e. sweep towards shorter wavelengths), the laser light and the resonance move in opposite direction and therefore the lineshape is compressed. Figure 2 shows these two possibilities with a conceptual sketch (main plot) and two experimental signals (insets) [31].

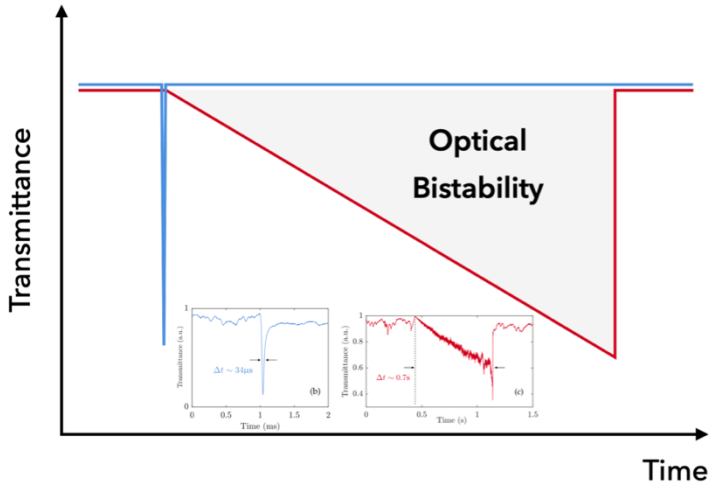

Fig 2. Sketch of the dynamical thermal behavior of a WGM resonance for a sweep towards longer wavelengths (red profile) and towards shorter wavelengths (blue profile). Blue inset: experimental signal showing the resonance narrowing Δt ~34 μs. Red inset: experimental signal showing the resonance broadening ~0.7 s.

If the laser sweep is stopped during the scan (for example at the half-point of the WGM fringe), a metastable warm-equilibrium is achieved and the detuning between the laser wavelength and the WGM resonance wavelength remains constant. This feature is very useful in practical terms, since it allows to compensate small perturbations and therefore to lock the system. Figure 3 illustrates with a conceptual sketch of this compensation mechanism, which is ultimately based on the change of the power circulating in the WGMR and its temperature. We start the argument by assuming to have centered the laser source on the blue side of the resonance (i.e. the fringe on the left side in Fig 3) [31].

When a small perturbation shifts the resonance toward longer wavelengths (i.e. to the right), the laser source becomes more off-resonance and therefore the coupled power decreases. This, in turn, decreases the WGMR temperature and moves the resonance towards shorter wavelengths (i.e. to the left), therefore compensating the initial perturbation (left panel of Fig 3). In the opposite scenario, where the small perturbation shifts the resonance toward shorter wavelengths (i.e. to the left), the inverse process

occurs. The perturbation shifts the resonance toward shorter wavelengths, the laser source becomes more in-resonance and therefore more power is coupled. This increases the MBR temperature and moves the resonance towards longer wavelengths (i.e. to the right), therefore compensating the perturbation (central panel of Fig 3) [32]. Since both mechanisms are based on the different positions of the laser source on the WGM fringe, the maximum shift that can be compensated is half of the resonance width (see right panel of Fig 3). In the case of more substantial shifts, the laser source goes completely off-resonance and the temperature compensation mechanism cannot trigger.

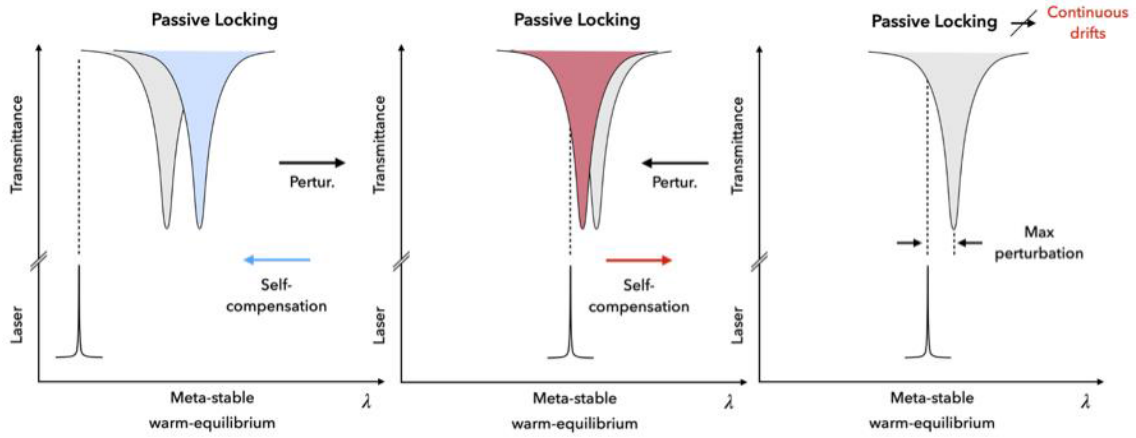

Fig 3. Self-compensation in the meta-stable equilibrium for cooling perturbations (left), heating perturbation (center), self-compensated maximum perturbation amplitude (right).

Finally, it is important to highlight that in some applications locking is not necessary and the WGM resonance is continuously and repetitively scanned [33]. In these cases, both the coupling power and the excitation wavelengths are not constants and this variability on a given range can help in achieving the phase matching condition for nonlinear effects. Since the nonlinear optical effects are much faster than the thermal effects, these two dynamics are typically separated in an experiment. On a more general note, however, the sweep velocity is set based on the input power, with faster sweeps for higher the inputs.

5 Optomechanical Effects

When a CW laser is tuned on the fringe of a WGM resonance and, in addition, it is locked on a specific point, a huge circulating power is confined into the WGMR. This high circulating power can induce not only nonlinear optical effects, but also mechanical oscillations due to the radiation pressure. Radiation pressure leads to the excitation of acoustic phonons, but these are of a different kind with respect to the ones of Stimulated Brillouin Scattering (SBS). In particular, SBS phonons are related to the microscopic structure of the material and fall in the GHz range for bulk silica, while the radiation-pressure phonons are related to the macroscopic shape of the resonator (i.e they are the mechanical eigenmodes of the cavity) and fall in the range of hundreds of kHz to tens of MHz for silica MBRs [12,34]. The oscillations induced by the radiation pressure are regenerative, exhibit a threshold and are triggered without an external modulation of the pump wave [35].

The oscillation of the resonance position produced by the optomechanical vibration leads to a periodic modulation of the system transmittance, as well as the formation of two sidebands separated by Ω_m from the central laser wavelength Ω_L. In analogy with the previous conventions, the blue shifted sideband ($\Omega_A = \Omega_L + \Omega_m$) is the anti-Stokes sideband, while the red-shifted sideband ($\Omega_A = \Omega_L - \Omega_m$) is the Stokes sideband. Figure 4 summarizes this process, which is referred to as the self-induced back-action Radiation

Pressure (RP) oscillation. Since WGM resonances have a Lorentzian profile, the sideband peaks are not equal in magnitude and, depending of the sign of the detuning, only one of them will be amplified. From this asymmetry either the damping or the amplification of the mechanical mode can happen (see Fig 5).

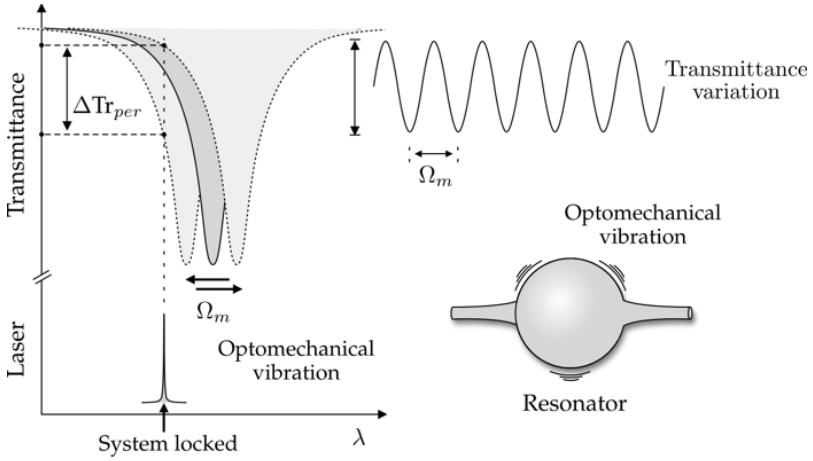

Fig 4. Illustration of the transmission modulation produced by the radiation-pressure optomechanical vibration W_m is assumed as the frequency of the mechanical eigenmode).

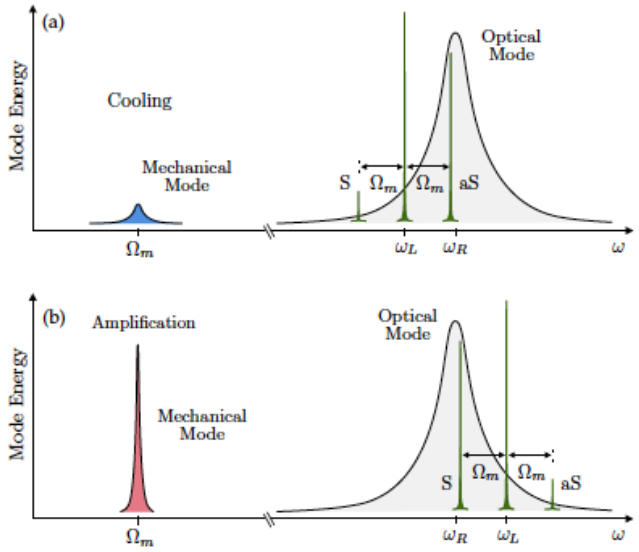

Fig 5. Sketch of the cooling and amplification of the mechanical mode: (a) enhancement of the anti-Stokes scattering, (b) enhancement of the Stokes scattering.

In general, when different optical nonlinearities are in competition, the one with the highest gain effectively triggers, while the others are suppressed. This general rule, which is a rephrasing of the energy conservation law, is partially bent in the case of RP oscillations, which indeed fall in the family of nonlinear optical effects. In fact, we have observed that RP oscillations can coexist with the parametrical and non-parametrical effects and, in particular, that the balance between the opto-mechanical effect and the parametrical/non-parametrical effects can be altered, even leading to the suppression of one side. This

balance is governed by the various aspects of the experimental configuration, such as the power circulating in the WGMR, the phase matching condition, the optical and mechanical Q factors of the resonances, the electromagnetic field distribution and the locked WGM resonance. To further highlight this coexistence, we point out that all the nonlinear effects described in this paper have been observed together with RP oscillations [12,36]. This leads to a straightforward consequence: the RP oscillation threshold is lower than the other ones and, therefore, the parametrical/non-parametrical processes appeared when the cavity was already vibrating.

After the pioneering work in toroids [36-38], the optomechanical oscillations have been observed in other WGMRs, such as spheroids [39,40], solid microbottles [41] and MBRs [12]. Finally, it was shown [36] that launching high input powers into toroids and spheroids produces an erratic behaviour, which is experimentally observed through the formation of period doubling [39]. A decade after this initial study, chaos mediated stochastic resonance and chaos transfer in a toroid were also demonstrated [43]. Despite of the interest in the temporal behavior of nonlinearities in WGMRs, the optomechanical chaotic behavior has remained largely unexplored experimentally and the study of the MBR by Roselló-Mechó *et al* [35] aimed at filling this gap for hollow WGMRs.

There is a great analogy among all WGMR, all works showed that the increase of pump power produced the same route to chaos. Indeed, the results indicate that RP induced chaotic motion is not limited to a special kind of WGMR, but it is an intrinsic property of the optical cavity [39].

The experimental setup (Fig 6) used for most of the experiments described here consists of a tunable laser source centered at 1550nm, and an erbium-doped fiber amplifier (EDFA). A small fraction of the launched signal was monitored to control the input power coupled into the WGMR. The light is then launched into a tapered fiber that will excite the WGM of the chosen resonator. Part of the output signal of the taper was sent to an optical spectrum analyser (OSA), and part into a fast photodetector (PD), connected either to an oscilloscope or to an electrical spectrum analyzer (ESA).

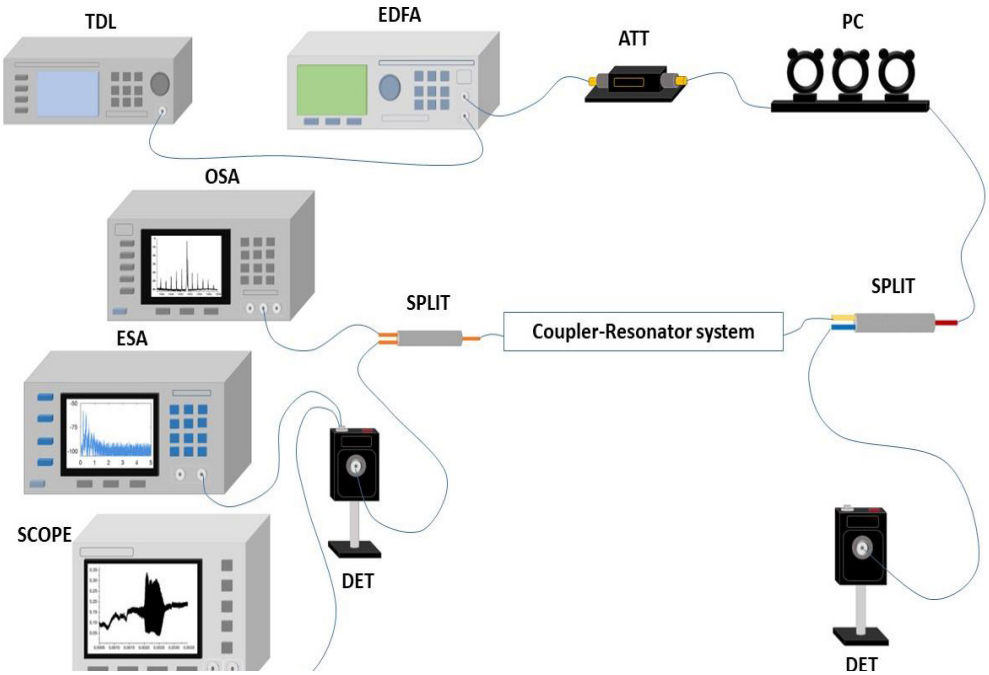

Fig 6. Scheme of the experimental setup employed to excite and measure the optomechanical vibrations induced by RP.

5.1 Optomechanical parametrical oscillations in toroids

Another type of WGM microcavity is constituted by a toroidally-shaped silica cavity supported by a silicon pillar on a microelectronic chip [43]. The toroidal shape of these resonators allows an extra level of geometric control with respect to spherical cavities. Their fabrication often uses oxide-coated Si wafers, and the process includes photolithography, wet and dry etching and laser reflowing. The laser reflowing is used to create a very smooth surface, as it effectively removes lithographic flaws; in this way, a Q as high as 4×10^8 at λ =1550 nm was achieved, together with a very small mode volume, approximately 180 mm^3 [44]. Figure 7, panel B, shows a render of the optomechanical oscillation in a toroid [37]. Rokhsari *et al* showed for the first time the radiation pressure instability in a toroidal microcavity, and the mechanical displacement of the torus [37]. The authors described a unique aspect of the microcavity: their fundamental mechanical breathing modes can exhibit high mechanical frequency at room temperature. In panel A, the authors showed the two family modes observed, the first and third flexural modes superimposed in the same graph. The inset and panel B show an exaggerated plot of the strain field and the mechanical oscillation that cause a displacement of the periphery of the toroid. These two distinct fundamental oscillations and their harmonics are plotted together.

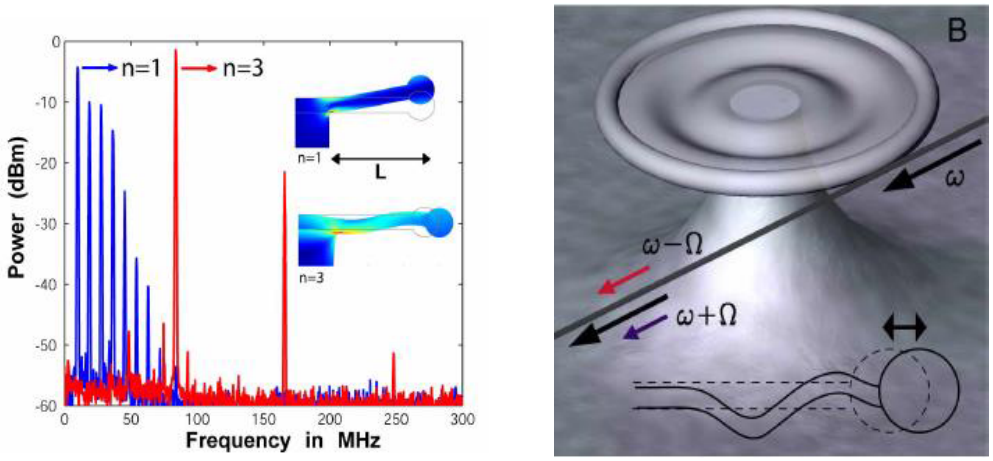

Fig 7. Panel A: Frequency of the vibration of the toroid measured with an electrical spectrum analyser. Two family of modes were observed, the n = 1 (blue line) and n = 3 (red line). The inset shows the modelled strain fields and the displacement caused by the mechanical oscillation. Panel B: A render of the high frequency vibration mode n = 3. Modified from [37].

Rokhsari *et al* [38] and Kippenberg *et al* [38] reported the simultaneous oscillation of several family modes in contrast to the Braginsky theory. Assuming that the authors were carefully setting the measurement in order to avoid aliasing, it could be possible to observe more than one mode oscillating simultaneously due to the fact that WGM microcavities have a very dense mode spectrum. The authors extended the coupled mode analysis of Braginsky to theoretically confirm that the mechanical oscillations they were observing are due to radiation pressure, ruling out thermal effects.

Figure 8 shows the calculated and measured field spectrum in the Fourier space (left panel). It was measured using a Fabry-Perot spectrometer with a 1 MHz linewidth. In the right panel, it shows the transmitted pump power versus time for two different input powers: 0.15 mW (onset of oscillations) and 5.8 mW.

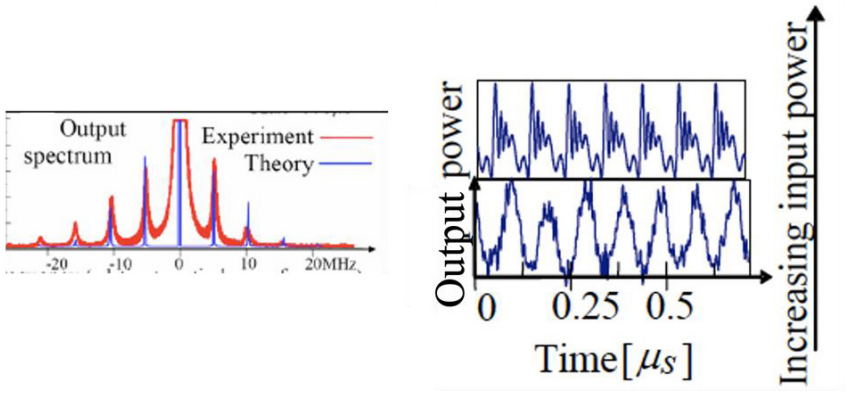

Fig 8. Left: Measured (red line) and calculated (blue line) spectrum of the transmitted optical power. Right: Transmitted pump power versus time for two different pump powers, 0.15 mW and 5.8 mW. Modified from [36].

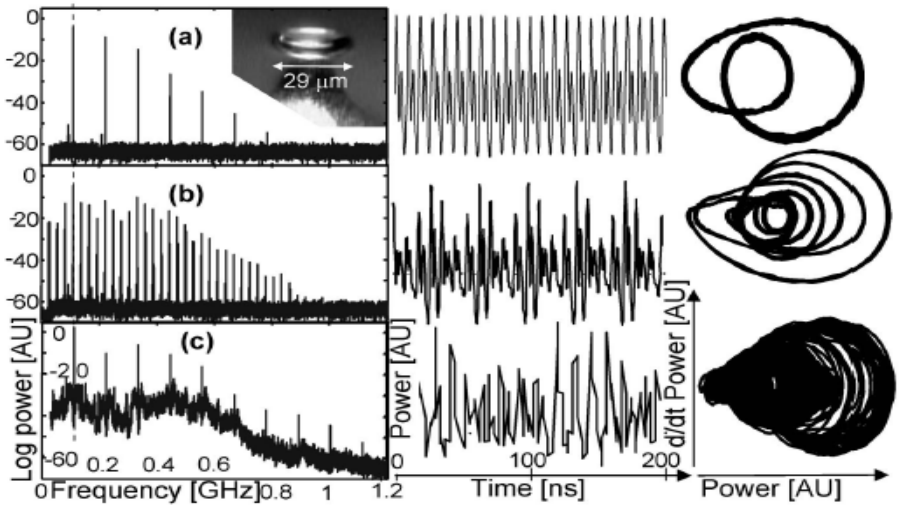

Fig 9. Experimental results in the frequency and time space are shown for three different pump powers: (a) 11 mW, (b) 21 mW and (c) 28.7 mW. Phase-space plots of the first derivative of the measured output power in time versus the measured output power are also shown. From [39].

Toroids are flexible structures and oscillate to lower frequencies compared to spheres, as we will see in the next subsection. The spectral evolution for the toroid starts with a periodic oscillation showing several harmonics, the appearance of two period doubling bifurcations (a period-four cycle) and a continuum superimposed to the fundamental frequency component and its high harmonics. Figure 9 shows this route to chaos in the frequency and time domain, together with their correspondent attractors. The toroid used in these experiments has a diameter of about 29 μm, an optical Q factor of 10^7 and a mechanical Q of about 250. For the subchaotic regime (pump power of 11 mW), the trajectories of two systems with infinitesimal differences in the initial conditions will not diverge. This is a limit-cycle dynamic, and it describes an attracting set to which trajectories converge and they are periodic. At higher input powers, when the oscillation is non-periodical, the regime is such that initially nearby points in phase space evolve into completely different

states. When the toroidal WGMR is slightly eccentric, the splitting of the spectral line could be observed. The calculation with COMSOL shows two mechanical eigenmodes that are rotated with respect to each other with a 0.25 MHz splitting between these rotated modes as a result of the perturbation (see Fig 10).

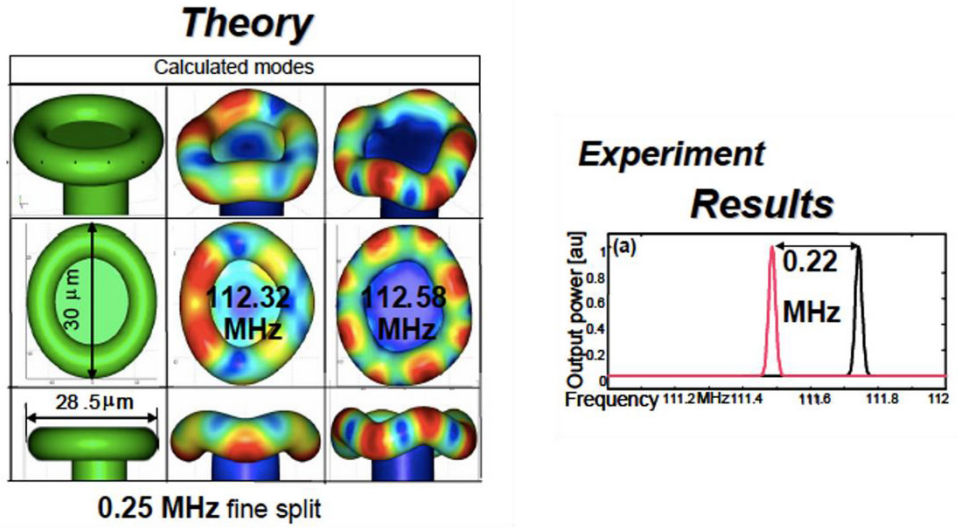

Fig 10. Left panel: Two degenerate modes calculated using COMSOL in color code, the modes are oriented with two different rotations. Right panel: experimental spectrum showing the spectral line splitting. Modified from [40].

Almost a decade later, Monifi *et al* [44] performed a detailed study of chaos transfer between a pump and a weak probe field using a toroidal WGMR. Their results showed that the probe also experienced periodic, quasi-periodic and chaotic regime through the same bifurcation route [45]. The authors demonstrated that both optical fields experienced period-doubling cascading for the same values of the pump power. The ratios of bifurcation intervals (a_1/a_2) are the same for both pump and probe fields and very close to the first universal Feigenbaum constant (4.6692), whereas the ratio between the width of a tine and sub-tine (b_1/b_2) are close to the second universal Feigenbaum constant (2.5029). The similar routes for the pump and probe fields can only be attributed to the optomechanical parametric oscillation of the WGMR.

5.2 Optomechanical parametrical oscillations in microspheres

In [39], Carmon *et al* showed the route to chaos using a solid spherical WGMR. Figure 11 shows the route to chaos that includes periodical oscillation for low input power, periodic doubling for medium power and a continuum for high input power. For this case, the microsphere has an optical Q of 7×10^6 and a mechanical Q of about 112. The silica microsphere is built onto a silicon chip [29] in order to increase the stiffness of the structure, which also pushes the vibration eigen frequencies to values in the GHz range. The frequency range of the oscillation is different from the toroidal WGMR.

The authors also showed they can selectively excite different modes by tuning the photon lifetime to be comparable with the acoustical period and performed modal spectroscopy. The position of the cavity will evolve according to the equation of motion for a mechanical oscillator, and it depends on the circulating optical power. The optical resonance shifts with the expansion of the structure. The dynamical behaviour was measured, and it resembled a sinusoidally moving Lorentzian line shape, as the Lorentzian deviation becomes larger, the system response becomes nonlinear. Figure 12 shows the measured oscillations and the calculated mechanical eigenmodes, the agreement between both is within 3%, mainly due to the simplification used for the COMSOL simulation.

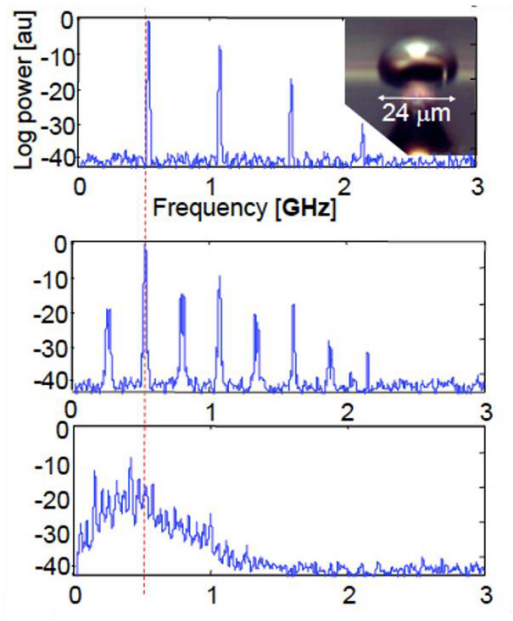

Fig 11. Oscillation spectra of a microsphere of about 24 μm in diameter for a pump power of 66 mW (upper graph) showing a periodical oscillation, 79 mW (middle graph) showing a periodical doubling of the oscillation and 83 mW (lower graph) showing a continuum. Modified from [39].

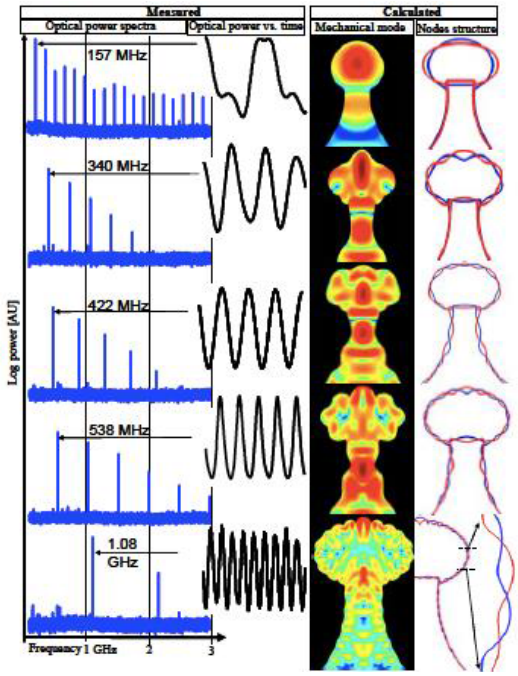

Fig 12. Measured amplitude oscillations with the corresponding mechanical modes in color code for the strain energy and the mode geometry. All deflections are exaggerated (Reproduced from [40]).

5.3 Optomechanical arametrical oscillations in microbbubles

MBRs also show a complex spectrum of mechanical modes. Ideally, these modes belong to different families. Radial breathing modes ($m = 0$) hold cylindrical symmetry corresponding to the extension-compression of the spherical shell across the longitudinal axis and are non-degenerate. Rocking modes ($m = 1$) correspond to a lateral bending of the MBR displaying double degeneracy with a mutual orientation of 90°. Wineglass modes ($m > 1$) are more balanced vibrations exhibiting more nodes and occasionally a sharp localization along the equatorial circumference of the MBR and maintaining double degeneracy at angles that depend on the order. However, most modes generated by the numerical solution exhibit an intricate shape that is hardly attributable to any major class. In the case of the MBR the influence of the capillary length cannot be neglected [12].

In particular, we tracked a few lowest energy breathing modes as well as a couple of higher energy modes in a regime of a few MHz displaying wineglass or hybrid profile, which were chosen for their strong localization along the equatorial circumference of the microbubble (in terms of elastic energy or strain), as well as an easily identifiable shape. The frequency of the lowest energy breathing modes scales with the number of nodes in the longitudinal oscillation of the capillary and does not depend much on the diameter of the microbubble. Instead, as a rule of thumb, we found that the natural frequency of the wineglass or hybrid structures around a few MHz approximately scales as $d_{microbubble}^{-a}$, where a typically falls in a range between 1 and 2. Figure 13 displays the effect of the diameter of the microbubble on a representative selection of mechanical modes.

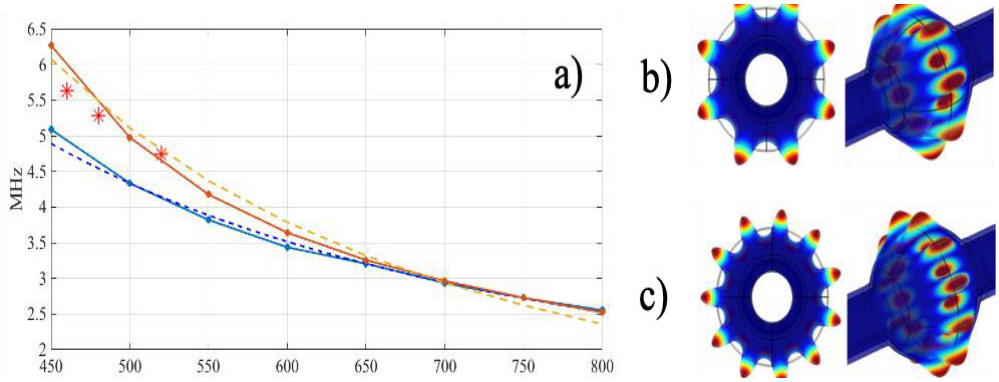

Fig 13. COMSOL Multiphysics® numerical simulations and experimental data. Effect of the diameter of the MBR on the excitation of the mechanical mode for (a) higher frequency modes displaying 11 (dark red, solid dots) or 8 nodes (blue circles), experimental data (stars) and fitting (red dashed line), (b) wine glass or hybrid mode with 8 nodes in plane and 3D view, (c) wine glass or hybrid mode with 11 nodes in plane and 3D view. Modified from [12].

The chaos route depicted in Fig 14 was measured for a MBR of 520 μm of diameter and wall thickness of about 4.2 μm. The fundamental mode oscillated at 4.74 MHz with a single series of harmonics for 200 mW of pump power (Fig 14a). At higher input powers, new frequencies arose in a quasi-periodic doubling (400 mW and 600 mW) till reaching a chaotic regime characterized by a continuum superimposed to the fundamental frequency component and its high harmonics. The authors also observed that for larger MBRs (diameters above 600 μm), the transition to chaos falls directly into continuum, skipping the sequences of discrete frequencies of quasi-period doubling [35].

Additionally, Roselló-Mechó *et al* performed a pump and probe characterization, and observed the same modulation frequencies and route to chaos [35]. This is a clear indication that the modulation is induced by true mechanical vibration of the MBR that is composed by all frequencies. The results are depicted in Fig 15.

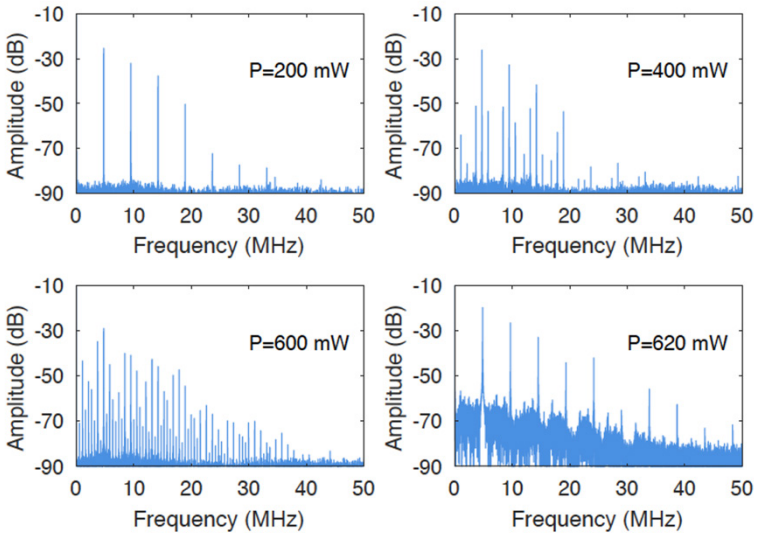

Fig 14. Route to chaos for a MBR of 520 µm of diameter and wall thickness of about 4.2 µm as the launched pump power is increased: (a) 200mW, (b) 400mW, (c) 600mW and (d) 620mW.

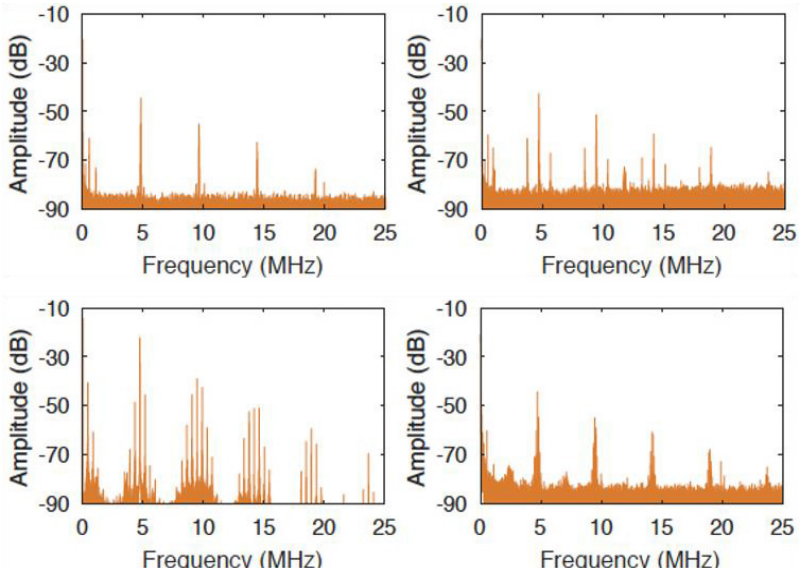

Fig 15. Route to chaos of the probe field (P =1mW) as the pump power was increased. Pump power (a) 200mW, (b) 400mW, (c) 600mW and (d) 620mW. MBR of 520 µm of diameter and wall thickness of about 4.2

6 Conclusion

We presented a review of experimental studies demonstrating radiation-pressure induced optomechanical oscillations in a WGMR, and their transition to a chaotic regime. The experiment were performed at room temperature using a continuous wave source and the chaotic vibration was reached without any external feedback or modulation. We have shown that the opto-mechanical oscillations (OMOs)

and the chaotic regime can be reached by WGMR of different sizes and shapes. For a particular type of WGMR, namely MBRs, two different routes to chaos are present, depending on the hollow resonator size. In particular, a quasiperiodic doubling for MBRs with diameters below 600 μm and an abrupt transition for bigger MBRs. The mechanical oscillations were observed as from the transmitted optical field as pure sinusoids, modulated sinusoids due to the presence of higher harmonics for all different WGMR described here and decaying ripples for the case of larger MBRs. We also showed that MBRs and toroidal WGMR can transfer chaos from a strong pump WGM to a very weak probe WGM through the mechanical motion and that the two signals follow the same route to chaos.

References

1. Maiman T, Stimulated optical radiation in ruby, *Nature*, 187(1960)493–494.
2. Franken P A, Hill A E, Peters C W, Weinreich G, Generation of optical harmonics, *Phys Rev Lett*, 7(1961)8; doi.org/10.1103/PhysRevLett.7.118.
3. Giordmaine J A, Miller R C, Tunable coherent parametric oscillation in linbo3 at optical frequencies, *Phys Rev Lett*, 14(1965)973; doi.org/10.1103/PhysRevLett.14.973.
4. Harris S E, Oshman M K, Byer R L, Observation of tunable optical parametric fluorescence, *Phys Rev Lett*, 18(1967)732; doi.org/10.1103/PhysRevLett.18.732.
5. Stolen R H, Ippen E P, Raman gain in glass optical waveguide, *Appl Phys Lett*, 22(1973)276–278.
6. Stolen R, Ashkin A, Optical kerr effect in glass waveguide, *Appl Phys Lett*, 22(1973)294–296.
7. Stolen R H, The early years of fiber nonlinear optics, *J Lightwave Tech*, 26(2008)1021–1031.
8. Frigenti G, Farnesi D, Conti G N, Soria S, Nonlinear Optics in Microspherical Resonators, *Micromachines*, 11(2020)303; doi.org/10.3390/mi11030303.
9. Lin G, Coillet A, Chembo Y K, Nonlinear photonics with high-Q whispering-gallery-mode esonators, *Adv Opt Photonics*, 9(2017)828–890.
10. Rayleigh L, The problem of the whispering gallery, *Phil Mag*, 20(1910)120; doi.org/ 10.1080 /147864 41008636993.
11. Suzuki R, Kato T, Kobatake T, Tanabe T, Suppression of optomechanical parametric oscillation in a toroid microcavity assisted by a kerr comb, *Opt Express*, 25(2017)28806–28816.
12. Rosello-Mecho X, Farnesi D, Frigenti G, Barucci A, Ratto F, Fernandez-Bienes A, Garcia-Fernandez T, Delgado-Pinar M, Andrés M, Conti G N, Soria S, Parametrical optomechanical oscillations in phoxonic whispering gallery mode resonators, *Sci Rep*, 9(2019)7163; doi.org/10.1038/s41598-019-43271-x.
13. Campillo A, Eversole J, Lin H, Cavity quantum electrodynamics enhancement of stimulated emission in microdroplets, *Phys Rev Lett*, 67(1991)437; doi.org/10.1103/PhysRevLett.67.437.
14. Chang R K, Campillo A J, (eds), Optical Processes in Microcavities, (World Scientific, Singapore), 1996.
15. Chiasera A, Dumeige Y, Feron P, Ferrari M, Jestin Y, Conti G N, Pelli S, Soria S, Righini, G, Spherical whispering-gallery-mode microresonators, *Laser & Photonics Reviews*, 4(2010)457–482.
16. Righini G, Dumeige Y, Feron P, Ferrari M, Conti N G, Soria S, Ristiı́C D, Whispering gallery mode microresonators: Fundamentals and applications, *Rivista del Nuovo Cimento*, 34(2011)435; doi.10. 1393/ncr/i2011-10067-2.
17. Righini G, Soria S, Biosensing by W G M microspherical resonators, *Sensors*, 16(2016)905; doi.org/10.3390/s16060905.
18. Sandoghdar V, Treussart F, Hare J, Lefevre-Seguin V, Raimond J M, Haroche S, Very low threshold Whispering-Gallery-Mode microsphere laser, *Phys Rev A*, 54(1996)1777; doi.org/10.1103/PhysRevA.54.R1777.
19. Kippenberg T J, Vahala K J, Cavity optomechanics, *Opt Express*, 15(2007)17172–17205.
20. Sumetsky M, Whispering gallery bottle microcavities: the three dimensional etalon, *Opt Lett*, 29(2004)8–10.
21. Berneschi S, Farnesi D, Cosi F, Conti G N, Pelli S, Righini G C, Soria S, High Q silica microbubble resonators fabricated by arc discharge, *Opt Lett*, 36(2011)3521–3523.
22. Ward J M, Yang Y, Chormaic S N, Highly sensitive temperature measurements with liquid-core microbubble resonators, *IEEE Phot Techn Lett*, 25(2013)23 2350–2353.

23. Ward J, Dhasmana N, Chormaic S N, Hollow core whispering gallery resonator sensors, *Eur Phys J, Special Topics*, 223(2014)1917–1935.
24. Bahl G, Kim K, Lee W, Liu J, Fan X, Carmon T, Brillouin cavity optomechanics with microfluid devices, *Nat Commun*, 4(2013)1994; doi.org/10.1038/ncomms2994.
25. Han K, Zhu K, Bahl G, Opto-mechano-fluidic viscometer, *Appl Phys Lett*, 105(2014)014103; doi.org/10.1063/1.4887369.
26. Frigenti G, Cavigli L, Fernández-Bienes A, Ratto F, Centi S, García-Fernández T, Conti G N, Soria S, Resonant microbubble as a microfluidic stage for all-optical photoacoustic sensing, *Phys Rev App*, 12(2019)01406; doi.org/10.1103/PhysRevApplied.12.014062.
27. Frigenti G, Cavigli L, Ratto F, Centi S, Murzina T V, Farnesi D, Pelli S, Soria S, Conti G N, Microbubble resonators for scattering-free absorption spectroscopy of nanoparticles, *Opt Express*, 29(2021)31130–31136.
28. Frigenti G, Arjmand M, Barucci A, Baldini F, Berneschi S, Farnesi D, Gianfreda M, Pelli S, Soria S, Aray A, Dumeige Y, Féron P, Conti G N, Coupling analysis of high Q resonators in add-drop configuration through cavityringdown spectroscopy, *J Opt*, 20(2018)065706; doi. 10.1088/2040-8986/aac459.
29. Vahala K J, Optical microcavities, *Nature*, 424(2003)839–846.
30. Gorodetsky M, Ilchenko V, Thermal nonlinear effects in optical whispering-gallery microresonators, *Laser Phys*, 2(1992)1004–1009.
31. Roselló Mechó X, Whispering Gallery Modes: Advanced Photonic Applications, Ph D Thesis, (2019), University of Valencia, URL https://www.educacion.gob.es/teseo/imprimirFicheroTesis.do?idFichero=Wge8ZCJAqfE\%3D.
32. Carmon T, Yang L, Vahala K, Dynamical thermal behavior and thermal self-stability of microcavities, *Opt Express*, 12(2004)4742–4750.
33. Vanier F, Rochette M, Godbout N, Peter Y.-A, Raman lasing in As_2S_3 high-Q whispering gallery mode resonators, *Opt Lett*, 38(2013)4966–4969.
34. Farnesi D, Righini G, Conti G N, Soria S, Efficient frequency generation in phoxonic cavities based on hollow whispering gallery mode resonators, *Sci Rep*, 7(2017)44198; doi.org/10.1038/srep44198.
35. Rosello-Mecho X, Frigenti G, Farnesi D, Delgado-Pina M, Andrés M V, Ratto F, Conti G N, Soria S, . Microbubble PhoXonic resonators: Chaos transition and transfer, *Chaos, Solitons & Fractals*, 154(2022) 111614; doi.org/10.1016/j.chaos.2021.111614.
36. Carmon T, Rokhsari H, Yang L, Kippenberg T J, Vahala K J, Temporal behavior of radiation-pressure-induced vibrations of an optical microcavity phonon mode, *Phys Rev Lett*, 94(2005)223902; doi.org/10.1103/PhysRevLett.94.223902.
37. Rokhsari H, Kippenberg T J, Carmon T, Vahala K J, Radiation-pressure-driven micro-mechanical oscillator, *Opt Express*, 13(2005)5293–5301.
38. Kippenberg T J, Rokhsari H, Carmon T, Scherer A, Vahala K J, Analysis of Radiation Pressure Induced Mechanical Oscillation of an Optical Microcavity, *Phys Rev Lett*, 95(2005)033901; doi.org/10.1103/PhysRevLett.95.033901.
39. Carmon T, Cross M C, Vahala K J, Chaotic Quivering of Micron-Scaled On-Chip Resonators Excited by Centrifugal Optical Pressure, *Phys Rev Lett*, 98(2007)167203; doi.org/10.1103/PhysRevLett.98.167203.
40. Carmon T, Vahala K J, Opto-Mechanical Modal Spectroscopy: Opto-Excited Vibrations of a Micron-Scale On-Chip Resonator, in Conference on Lasers and Electro-Optics/Quantum Electronics and Laser Science Conference and Photonic Applications Systems Technologies, OSA Technical Digest (CD) (Optica Publishing Group, 2007), paper JMB2.
41. Asano M, Takeuchi Y, Chen W, Ozdemir S K, Ikuta R, Imoto N, Yang L, Yamamoto T, Observation of optomechanical coupling in a microbottle resonator, *Laser Photonics Rev*, 10(2016)603–6011.
42. Monifi F, Zhang J, Özdemir Ş, Peng B, Liu Y, Bo F, F Nori F, Yang L, Optomechanically induced stochastic resonance and chaos transfer between optical fields, *Nat Photon*, 10(2016)399–405.
43. Armani D K, Kippenberg T J, Spillane S M, Vahala K J, Ultra-high-q toroid microcavityon a chip, *Nature*, 421(2003)925–928.
44. Kippenberg T J, Spillane S M, Vahala K J, Demonstration of ultra-high-q small mode volume toroid micro-cavities on a chip, *Appl Phys Lett*, 85(2004)6113–6115.

45. Bakemeier L, Alvermann A, Fehske H, Route to chaos in optomechanics, *Phys Rev Lett*, 114(2015) 013601; doi. org/10.1103/PhysRevLett.114.013601.

[*Received*: 15.12.2023; *accepted*: 25.12.2023]

Silvia Soria received the M Sc and Ph D degrees in Physics from the University of Barcelona, Spain, in 1994 and 1999, respectively. She worked as a postdoctoral researcher at Laser Laboratorium Goettingen e.V., in Germany. She was a Ramon y Cajal fellow at ICFO-Institute of Photonics Science in Barcelona, Spain. Currently she is a senior researcher at IFAC- N. Carrara Institute of Applied Physics, of the Italian CNR and a habilitated Professor in Applied Physics. Her areas of research include lasers, non-linear optics, soft matter and biophotonics. She has authored over 100 publications and presented her results in many international congresses. She is a member of the committee of Equal Opportunities at the Italian Society of Physics and Editor in chief at JEOS-RP.